UNCONDITIONALLY STABLE SPLITTING METHODS FOR THE SHALLOW WATER EQUATIONS

RUNAR HOLDAHL, HELGE HOLDEN, AND KNUT-ANDREAS LIE

Abstract. The front tracking method for hyperbolic conservation laws is combined with operator splitting in order to study the shallow water equations. Furthermore, the method includes adaptive grid refinement. The front tracking method is unconditionally stable, but for practical computations feasible CFL numbers are moderately above unity (typically between 1 and 5). The method resolves shocks sharply and is highly efficient.

The numerical technique is applied to four test cases, the first being an expanding bore with rotational symmetry. The second problem addresses the question of describing the time-development of two constant water levels separated by a dam that breaks instantaneously. The third problem compares the front tracking method with an explicit analytic solution of water waves rotating over a parabolic bottom profile. Finally, we study flow over an obstacle in one-dimension.

1. Introduction

The shallow water equations model free surface flow for a fluid under the influence of gravity in the case where the vertical scale is assumed to be much smaller than the horizontal scale. They can be derived from the depth averaged incompressible Navier–Stokes equations and express conservation of mass and momentum. The shallow water equations have applications to a wide range of phenomena other than water waves, e.g., avalanches [24] and atmospheric flow [7]. In the case of free surface flow when the shallow water approximation is not valid, it is common to model the surface waves using several layers of shallow water equations coupled via the pressure, [17, 18, 21, 29, 30]. Furthermore, the shallow water equations coincide with the Euler equations of gas dynamics in the case of isentropic gas flow with $\gamma = 2$. Thus the 2×2 shallow water equations often serve as a simpler test case compared with the full 3×3 system of Euler equations.

Front tracking is a powerful tool to analyze systems of strictly hyperbolic conservation laws in one space dimension. It can briefly be described as follows. We make the standard approximation of the initial data by a piecewise constant function. Due to the finite speed of propagation in hyperbolic systems, the initial value problem is reduced to a family of Riemann problems, i.e., isolated jumps separating two constant states. If the two states are close, the solution of the Riemann problem can be described by the Lax construction. Thus the solution consists of a combination of at most n elementary waves, i.e., shocks,

Date: April 16, 1998.

1991 *Mathematics Subject Classification.* 65M12, 65M50, 76B15, 35L65.

Key words and phrases. Front tracking, operator splitting, grid refinement, shallow water equations.

The third author has been supported by grant 100555/410 from the Norwegian Research Council.

contact discontinuities, or rarefaction waves. In the front tracking approximation shocks and contact discontinuities are unchanged while the rarefaction wave is approximated by sampling points along the wave. In this way we get a piecewise constant solution. We denote the discontinuities as fronts. When fronts collide, new Riemann problems are created which are solved in the same manner.

As the approximation of the initial data improves and the number of points on rarefaction waves increase, the approximate solution converges to a solution of the initial value problem, see Risebro [25]. This result holds when the system is strictly hyperbolic and the initial data has small total variation.

Recently the wave-front tracking method of Bressan *et al.*, closely related to the front tracking method just described, has been shown to yield uniqueness and stability of solutions, a major breakthrough in the theory of systems of conservation laws. See [4] and [5].

Front tracking as we have described it so far, is restricted to one spatial dimension. The extension to multidimensional systems is accomplished by dimensional splitting where the solution is obtained in one spatial direction at the time, then projected onto a grid before the equation is solved in the other spatial directions. In the inhomogeneous case we use operator splitting to handle the source term.

For other numerical implementations of the front tracking method for hyperbolic systems we refer to [26, 27, 12, 13, 8]. In particular, [8] involves similar numerical methods applied to the Euler equations of gas dynamics. Here we apply front tracking as a numerical technique to the shallow water equations. It is tested on four test cases.

The first case concerns the collaps of an elevated circular region of water. The rotational symmetry of the problem allows for testing of possible grid effects. Front tracking is compared with three second order, unsplit methods; the non-oscillatory central schemes of Jiang and Tadmor [11], the composite CFLF4 method of Liska and Wendroff [19, 20], as well as the CLAWPACK code of LeVeque [14]. While Jiang and Tadmor's method and the CFLF4 method are based on central differences, the wave propagation method of CLAWPACK and front tracking are based on the solution of Riemann problems. All methods show slight distortions due to the Cartesian grid. Front tracking is run at considerably higher CFL numbers than the other methods. To give a stable solution Jiang and Tadmor's method requires very small CFL numbers, making the method slow. Front tracking and CLAWPACK resolve the leading shock very sharply, CLAWPACK gives best approximation of the dip following the shock, while front tracking resolves the sonic point accurately. Front tracking is considerably faster than the other methods. See [23, 29] for alternative numerical methods applied to the same problem.

The second problem models the breaking of a dam, see [1, 2, 3, 6] for earlier treatments of this problem. More precisely, we have two different levels of water separated by a dam which is assumed to break instantaneously. Compared with methods described in [1, 2, 3, 6] front tracking is considerably less diffusive. We have also implemented one level of adaptive grid refinement, see [8, 16]. By including grid refinement for this problem, we achive high accuracy with a reduced computational cost.

The third problem addresses the question of describing the motion of water waves on a parabolic bottom, comparing with an explicit solution due to Thacker [28]. The solution describes a planar water surface that rotates. Here the equations are inhomogeneous, and the source term is treated using operator splitting. The front tracking method shows excellent agreement with the exact solution. A convergence study verifies the first order convergence of the method.

While the previous three problems are two-dimensional, the last problem treats flow over an obstacle in one spatial dimension. To treat the resulting source term in the equations we employ an operator splitting. The simulations are compared with a composite scheme of Liska and Wendroff, see [19]. Sharp resolution of shocks (within *one* grid cell) is obtained by including an adaptive, shock-tracking grid.

2. Front Tracking and Dimensional Splitting

Let the strictly hyperbolic conservation law be given by

$$U_t + f(U)_x = 0, \quad U|_{t=0} = U_0. \tag{1}$$

When we approximate U_0 by a piecewise constant function $U_{0,\delta}$, where δ measures the approximation, the initial value problem (1) is reduced to a family of Riemann problems that will be solved separately. Consider a Riemann problem with left state U_L and right state U_R. The solution can be written as a combination of at most n elementary waves. Shock waves and contact discontinuities remain unchanged. Assume that a rarefaction wave from the jth family connects states U_l and U_r, that is,

$$U_r = \mathcal{R}_j(U_l; \epsilon_j),$$

for some ϵ_j, where $\mathcal{R}_j(U;\cdot)$ is the jth rarefaction curve from (left) state U. Define $M = \lceil(\lambda_j(U_r) - \lambda_j(U_l))/\delta\rceil$, where $\lambda_j(U)$ denotes the jth eigenvalue of $f'(U)$. Furthermore, let $\tilde\delta = (\lambda_j(U_r) - \lambda_j(U_l))/M$. We replace the rarefaction wave by the step function

$$U(x,t) = \begin{cases} U^0 = U_l & \text{for } x \le \xi_1 t, \\ U^1 & \text{for } \xi_1 t \le x \le \xi_2 t, \\ \vdots & \\ U^k & \text{for } \xi_k t \le x \le \xi_{k+1} t, \\ \vdots & \\ U^{M-1} & \text{for } \xi_{M-1} t \le x \le \xi_M t, \\ U^M = U_r & \text{for } x \ge \xi_M t. \end{cases}$$

Here

$$U^k = \mathcal{R}_j(U_l; k\tilde\delta), \qquad \xi_k = \frac{1}{2}(\lambda_j(U^k) + \lambda_j(U^{k-1})).$$

The resulting approximate solution is a piecewise constant function which we denote by U_δ. Moreover, we denote discontinuities by *fronts*. When fronts collide, new Riemann problem appear that are solved in the same manner. In general there will be a build-up of the number of fronts. To avoid an infinite number of fronts in finite time, we perform a data reduction by removing small waves. We measure the size of a wave by the variation of the wave divided by the number of components that are non-constant over the wave. The cut-off level of small waves is predetermined by the user, see [12].

Front tracking as we have described it, is a one-dimensional method, and the extension to multi-dimensional problems is accomplished by dimensional splitting. In this approach we introduce a rectangular Cartesian grid, and solve the hyperbolic conservation law in "tubes" in one spatial direction. The solution is then projected onto the grid, and the conservation law is subsequently solved in tubes in the next spatial direction followed by a projection onto the grid. The procedure is repeated in all spatial directions. In the scalar case, this method is well understood, and one can prove that the method converges to the right solution [9] and derive a priori error estimate [16].

To allow for finer resolution near shocks we have implemented an adaptive grid refinement based on the method described in [16]. In the projection phase, coarse grid cells are refined whenever the variation within a grid cell in the direction we are solving exceeds a predefined value. Similarly, in a postprocessing phase we determine the variation over all refined cells within each underlying coarse cell, and if the total variation is less than a given value, we return to the original coarse grid in that cell. By adopting this strategy, the projection error in each time step is reduced, and the accuracy is enhanced. It is important to notice that no local time stepping is required. Furthermore, the method is strictly local, and no patching of refined regions is performed. Only one level of refinement is currently implemented. For more details we refer to [16].

Boundaries are treated as fronts with a special identifying tag that allows the code to treat collisions between fronts without taking into account if a front is part of a boundary or not. Moving fronts are thus easily implemented. See [12, 8].

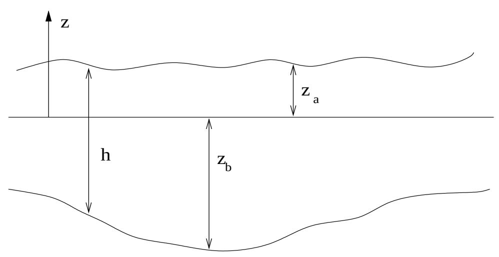

FIGURE 1. The quantities involved in the shallow water equations.

3. Governing Equations

The shallow water equations describe free surface flow for a fluid under the influence of gravity when the height of the top surface above the bottom is sufficiently small compared with some characteristic length of motion. In particular, vertical motion is ignored, and we have hydrostatic balance in the vertical direction.

We may write the shallow water system as the following nonhomogeneous system of conservation laws

$$
\begin{pmatrix} h \\ hu \\ hv \end{pmatrix}_t + \begin{pmatrix} hu \\ hu^2 + \frac{1}{2}gh^2 \\ huv \end{pmatrix}_x + \begin{pmatrix} hv \\ huv \\ hv^2 + \frac{1}{2}gh^2 \end{pmatrix}_y = \begin{pmatrix} 0 \\ -gh\frac{\partial z_b}{\partial x} \\ -gh\frac{\partial z_b}{\partial y} \end{pmatrix}. \tag{2}
$$

Here h denotes water depth, u and v are depth-averaged velocities in the x and y directions, respectively, and g is the acceleration of gravity. The right-hand side of (2) models the influence of a variable bottom. Figure 1 illustrates the situation and the quantities involved. The function $z_b = z_b(x,y)$ describes the bottom topography while $z_a = z_a(x,y,t)$ models the water surface elevation, and we have that $h = z_a - z_b$.

The Riemann problem for the shallow water equations in the one-dimensional homogeneous case can be solved explicitly. The system is strictly hyperbolic, and genuinely nonlinear in both families. The rarefaction waves read

$$
u = \begin{cases} u_l - 2(\sqrt{h} - \sqrt{h_l}) & \text{for the first family with } 0 < h < h_l, \\ u_l + 2(\sqrt{h} - \sqrt{h_l}) & \text{for the second family with } h > h_l, \end{cases} \tag{3}
$$

for a fixed left state (u_l, h_l). The Lax shock curves are given by

$$
u = \begin{cases} u_l - \frac{1}{\sqrt{2}}(h - h_l)\sqrt{h^{-1} + h_l^{-1}} & \text{for the slow shock with } h > h_l, \\ u_l + \frac{1}{\sqrt{2}}(h - h_l)\sqrt{h^{-1} + h_l^{-1}} & \text{for the fast shock with } 0 < h < h_l. \end{cases} \tag{4}
$$

The "vacuum case" $h = 0$ can be incorporated in the solution, see [22, 10]. In the next section we present some numerical solutions of (2) computed by front tracking.

4. Numerical Results

In this section we solve four different problems in shallow water hydrodynamics by the front tracking algorithm. The first two problems are homogeneous, while the bottom profile is varying in the last two examples such that the governing equations are nonhomogeneous. The numerical solutions are compared with both exact solutions and solutions computed by other numerical methods. These methods are

LWLF4	–	One-dimensional composite scheme consisting of three Lax–Wendroff steps followed by a Lax-Friedrichs step [19].
CFLF4	–	Composite scheme consisting of three steps with a second order predictor-corrector method followed by a Lax-Friedrichs step [19, 20].
JT	–	Second order, central difference scheme [11].
CLAWPACK $T^{2,2}$	–	Wave propagation method from the software package CLAWPACK [14]. The method is second order with transverse propagation of both increment waves and correction waves.

CLAWPACK is implemented in FORTRAN, while we coded the other three methods in C.

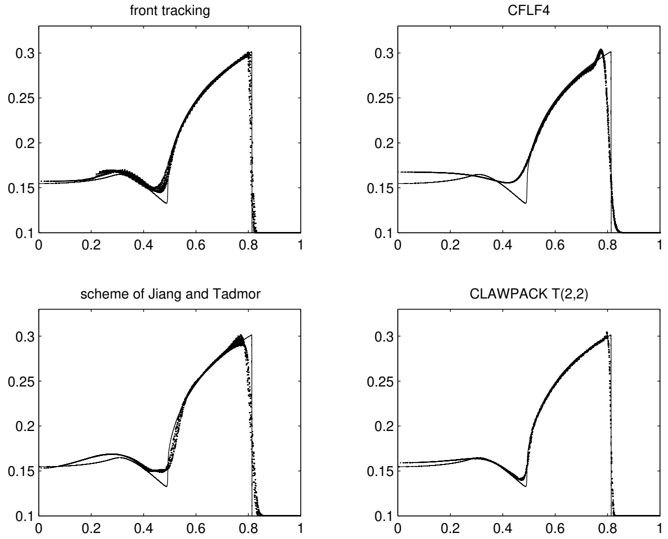

FIGURE 2. Water surface elevation for the explosion problem at time $t = 0.19$. The solid line is the radially symmetric solution.

4.1. **Explosion problem.** To test the accuracy of the front tracking and dimensional splitting algorithms with respect to grid orientation effects we try to solve a rotational symmetric problem on a Cartesian grid. We compare the front tracking method with the unsplit methods JT, CFLF4 and CLAWPACK $T^{2,2}$. A radially symmetric solution on a very fine grid is also computed, and this solution can be regarded as a very good approximation to the true solution.

The explosion problem considered here has initial data that consists of two constant states separated by a circle,

$$\begin{aligned} h(x,y,0) &= \begin{cases} 1.0, & \sqrt{x^2+y^2} \leq 0.3, \\ 0.1, & \text{otherwise}, \end{cases} \\ u(x,y,0) &= v(x,y,0) = 0. \end{aligned}$$

We assume absorbing boundary conditions. The solution consists of an expanding circular shock wave. Within the shock there is a rarefaction wave transporting water from the original deep region out to the shock. In the numerical computations the domain is $[-1.0, 1.0] \times [-1.0, 1.0]$ with absorbing boundary conditions. For all methods a uniform Cartesian grid with 160 grid cells in each direction was used. The initial data was approximated by taking the spatial average over each grid cell.

Scatter plots of the water surface elevation at time $t = 0.19$ are shown in Figure 2, while Figure 3 shows the corresponding plots of the radial velocity. In both figures the radially symmetric solution is represented by a solid line. s are displayed in Table 4.1 together with the CPU time used in each computation. The CPU times cannot be compared directly since the numerical schemes have not been optimized, but they should give an indication

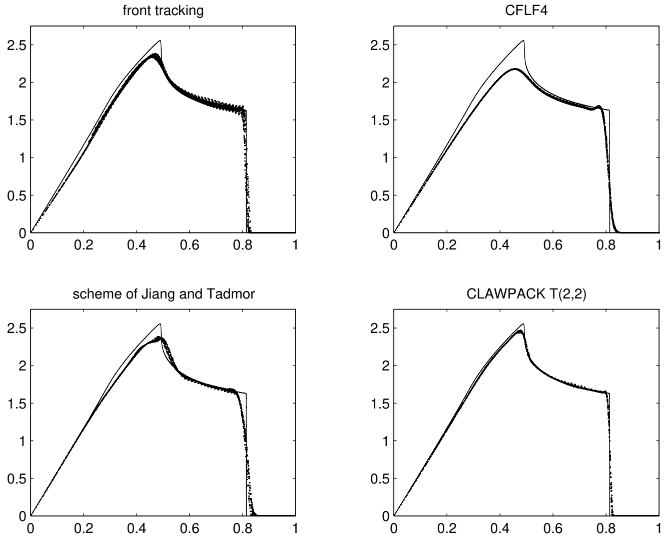

FIGURE 3. Velocity distribution for the explosion problem at time $t = 0.19$. The solid line is the radially symmetric solution.

TABLE 1. CFL numbers and CPU times for the explosion problem.

method	CFL number (fixed)	CPU time (normalized)
front tracking	1.50	1.0
CFLF4	0.40	4.7
JT (MM_2-limiter)	0.10	84.7
CLAWPACK $\mathrm{T}^{2,2}$ (MC-limiter)	0.90	15.1

of the efficiency of the various methods. In Table 4.1 we notice in particular the low CFL number used for JT. At higher CFL numbers this method did not show proper convergence near the origin. For instance, at the origin the solution dropped down to approximately 0.1 in a computation with a CFL number of 0.475. Computations with the MM_1-limiter and UNO-limiter did not improve the numerical results.

As far as computational time is concerned, front tracking and CFLF4 were most efficient, and the other methods were considerably slower. Partly due to the low CFL number, JT was very inefficient on this problem.

From the plots of the surface elevation we see that the front tracking solution gives a sharp resolution of the shock and corresponding peak. The same is true for CLAWPACK $\mathrm{T}^{2,2}$. For the last two methods, excessive smearing is observed and the upper part of the peak is cut off. In addition, CFLF4 has an overshoot near the discontinuity. This overshoot is probably caused by the second order predictor-corrector method used in the composite scheme. Also JT and CLAWPACK $\mathrm{T}^{2,2}$ overshoot the peak to some extent.

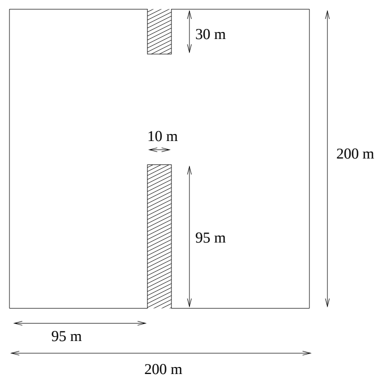

FIGURE 4. The reservoir.

The rarefaction wave is well approximated by all methods, except JT. On the other hand, only CLAWPACK $\mathrm{T}^{2,2}$ was able to resolve well the minimum point at $x \approx 0.5$. Also the radially symmetric solution converged slowly in this region. Furthermore, we notice that front tracking gives the best approximation near the sonic point at the origin.

The same remarks as above can be made about the scatter plots of the velocity in Figure 3. Here we notice in particular that CLAWPACK $\mathrm{T}^{2,2}$ is superior in resolving the rarefaction wave and the peak.

The scatter plots show that all solutions are influenced by the underlying Cartesian grid. However, CLAWPACK $\mathrm{T}^{2,2}$ preserves the symmetry very well. CFLF4 also has rather good symmetry properties. In the front tracking solution the grid orientation effects are more noticeable, which is to be expected since this method is the only splitting method of the four.

4.2. **Dambreak problem.** Here we discuss a problem reported in [1, 2, 3, 6]. Consider a 200m long and 200m wide reservoir with two different constant levels of water separated by a dam. At $t = 0$ part of the dam breaks instantaneously. The dam is 10m thick and the breach is assumed to be 75m wide. Figure 4 shows a sketch of the reservoir. The initial conditions are given by

$$\begin{aligned} h(x,y,0) &= \begin{cases} 10, & x \le 100 \\ 5, & \text{otherwise}, \end{cases} \\ u(x,y,0) &= v(x,y,0) = 0. \end{aligned}$$

In the references mentioned above the solution is displayed at time $t = 7.2$s, but to illustrate how the solution evolves in time we have shown the solution at times $t = 3.6$s, 7.2s, and 10.8s in Figure 5. In the left column the water surface elevation is plotted, while the right column contains the corresponding contourplots. All computations are made on a uniform Cartesian grid with 40×40 grid cells and a fixed CFL number of 1.5. Initially the solution consists of a bore propagating into the downstream side of the reservoir while spreading laterally. At the same time a rarefaction wave travels to the left. In the second plot in

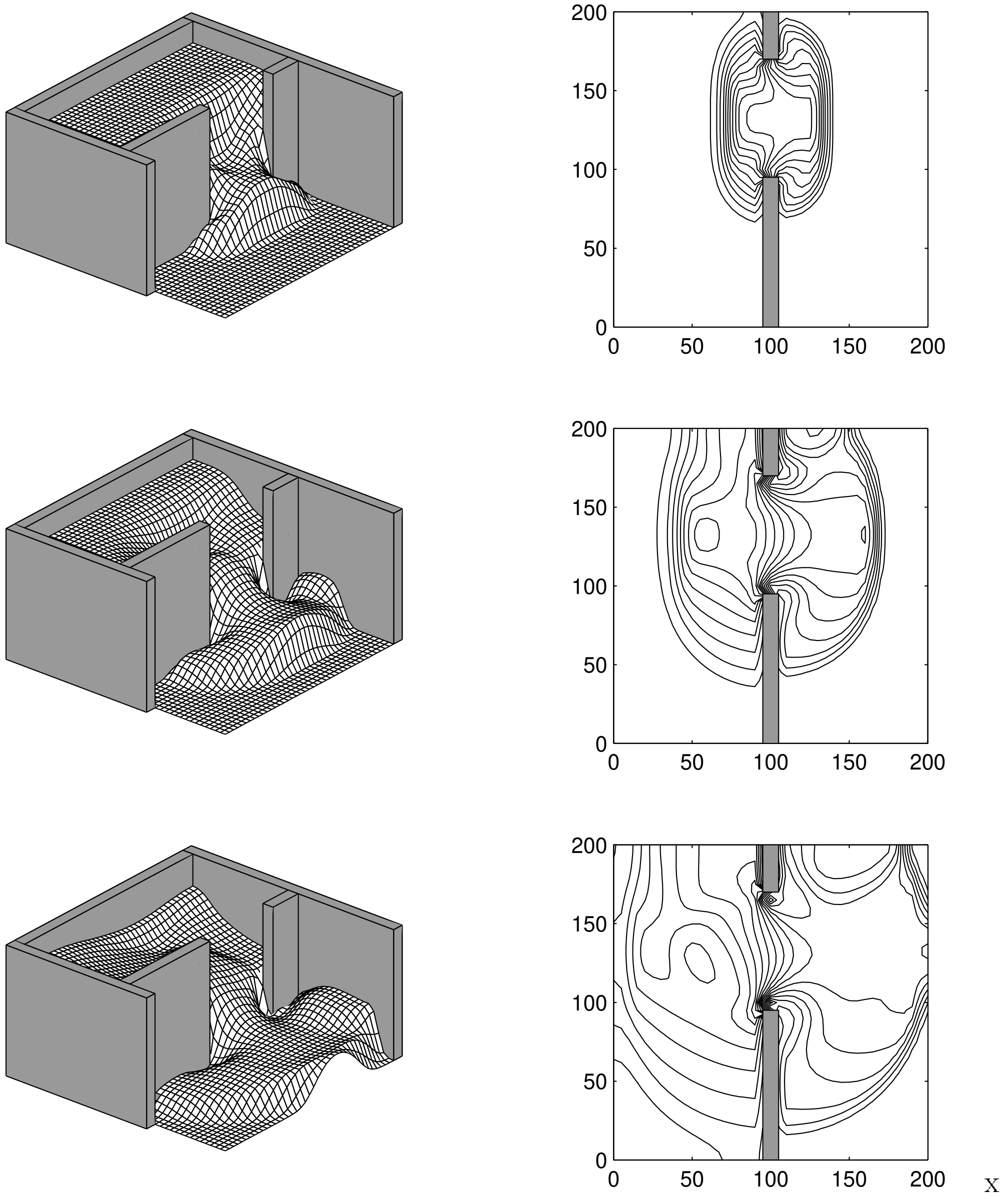

FIGURE 5. Water surface elevation for the dambreak problem at times $t = 3.6$s, 7.2s, 10.8s.

Figure 5 the bore has been reflected from one of the side walls of the reservoir and in the third plot the bore has just reached the wall in the downstream direction of the dam.

Compared with the numerical solutions computed in the references, the front tracking solution is less diffusive than both the first order method in [3] and the second order methods in [1, 2, 6]. The front part of the bore is resolved by 2 grid points using front tracking, while approximately 4 points are required by the second order methods. The

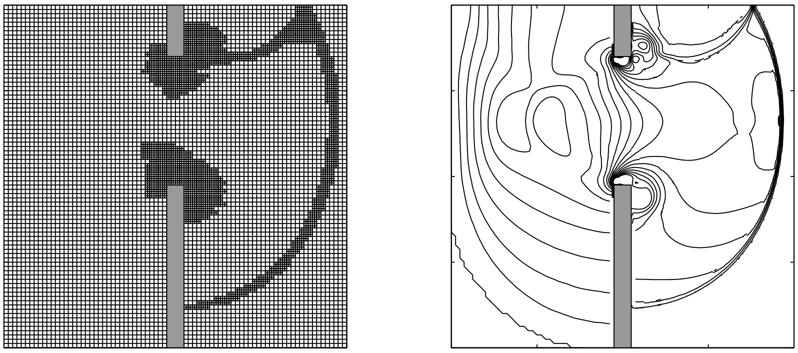

FIGURE 6. Grid in final step and contourplot for the dambreak problem at time $t = 10$s using grid refinement on a 80×80 grid.

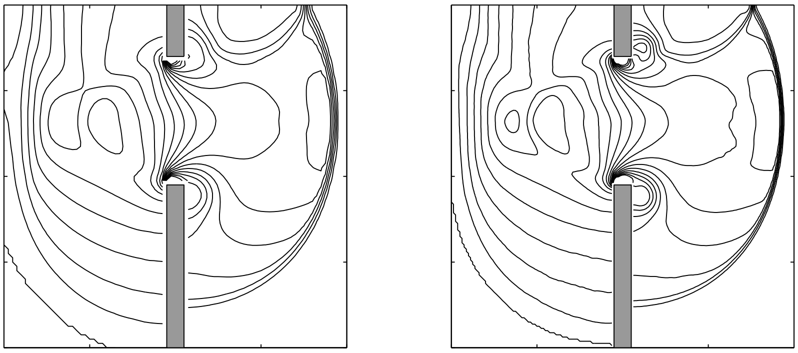

FIGURE 7. Contourplots for the dambreak problem at time $t = 10$s computed on a 80×80 grid (left) and a 160×160 grid (right).

first order method is even more diffusive. Furthermore, in regions where the solution is smooth, the front tracking solution looks very similar to the ones obtained by the second order methods. In particular, the contourplot is almost the same as the one produced by the second order method in [1].

To resolve the dynamics of the problem satisfactory we have to use a certain minimum of time steps in the splitting method. For the relatively coarse (40×40) grid used above this minimum corresponds to a low CFL number of 1.5. However, numerical tests on finer grids showed that the CFL number could typically be increased up to 4–5 without reducing the quality of the solution. In fact, increasing the CFL number gives sharper resolution of shock waves. The same has been observed for the Euler equations [8].

4.3. **Dambreak problem with grid refinement.** We have tested the adaptive grid refinement on the dambreak problem of the previous section. In the numerical calculations a local refinement factor 2 was chosen in each direction and one level of refinement was used. The underlying coarse grid had 80×80 cells and we used threshold parameters $(\mathrm{TV}_{\min}, \mathrm{TV}_{\max}) = (2.5, 5.0)$ in the adaption algorithm, see [8]. Figure 6 shows the grid and

TABLE 2. CPU times for the dambreak problem with grid refinement.

grid	refinement	CPU time (normalized)
80×80	yes	3.5
80×80	no	1.0
160×160	no	5.7

a contourplot of the surface elevation at time $t = 10$s. For comparison Figure 7 contains contourplots of the surface elevation computed on a 80×80 and a 160×160 grid without refinement. In all computations the CFL number was 1.5. All details in the solution on the 160×160 grid are captured by using the refinement. The weak wave reflected from the upper wall is even slightly sharper in Figure 6.

Table 2 contains the CPU times for three computations and shows that a gain in efficiency can be obtained by using grid refinement. We have performed several computations which show that the gain increases as the number of cells in the underlying grid increases. Moreover, while the dimensional splitting code is rather optimally designed, further improvements could probably be obtained by optimizing the grid refinement code.

4.4. **Time dependent motion in a parabolic basin.** There are not many exact solutions of the shallow water equations available, especially not for the case when the boundaries between water and dry land are moving. But in an article by Thacker [28] some exact solutions for shallow water flow in a parabolic basin are presented. The motion corresponds to normal mode oscillations for which the water surface rotates in the basin. For one of the solutions the water surface remains planar at all times. Here we compare this particular solution with the solution computed by front tracking. Since the bottom profile is variable, a source term is present on the right hand side in the shallow water equations. To handle this term we use operator splitting. The source term only depends on the spatial variables x and y, and hence the resulting ordinary differential equation can be solved exactly.

In this example it is most convenient to work in nonconservative variables z_a, u and v. If we take $g = 1$, the shallow water equations can be written as

$$\begin{aligned}
\frac{\partial z_a}{\partial t} + \frac{\partial}{\partial x}\left[(z_a - z_b)u\right] + \frac{\partial}{\partial y}\left[(z_a - z_b)v\right] &= 0, \\
\frac{\partial u}{\partial t} + u\frac{\partial u}{\partial x} + v\frac{\partial u}{\partial y} + \frac{\partial z_a}{\partial x} &= 0, \\
\frac{\partial v}{\partial t} + u\frac{\partial v}{\partial x} + v\frac{\partial v}{\partial y} + \frac{\partial z_a}{\partial x} &= 0.
\end{aligned}$$

Furthermore, we assume that the bottom profile is parabolic, i.e.,

$$z_b(x, y) = D_0\left(\frac{x^2 + y^2}{L^2} - 1\right).$$

Under these assumptions Thacker found two basic solutions where the water surface remains planar and the velocities vary sinusoidally with time

$$\begin{aligned} z_a &= 2A\frac{D_0}{L}\left(\frac{x}{L}\cos\omega t \pm \frac{y}{L}\sin\omega t + B\right), \\ u &= -A\omega\sin\omega t, \\ v &= \pm A\omega\cos\omega t, \\ \omega &= \sqrt{\frac{2D_0}{L^2}}. \end{aligned}$$

A is here a constant that determines the amplitude of the motion, B determines the reference level and ω is the frequency. Since the shallow water equations are based on the assumption of a hydrostatic pressure distribution, the vertical acceleration must be negligible compared with g. The solutions are therefore only valid when $A \ll L^2/2D_0$.

For the numerical computations we have chosen the positive sign and $A = L/2$, $B = -A/2L$, $D_0 = 1$, $L = 2500$. Computations were made on a uniform Cartesian grid with 101 grid cells in each direction. Numerical and exact solutions along the plane $y = 0$ at different times during the first period of the oscillation are shown in Figure 8. Figure 9 displays the water level $h = z_a - z_b$ at three different locations along the plane $y = 0$. For the computations in Figure 8 we have used a fixed CFL number of 1.25, while in Figure 9 we have chosen a fixed time step $\Delta t = 55.5$. From Figure 8 we see that the numerical solutions approximate the exact solution quite well. Some inaccuracies are noticeable along the shoreline. The second figure also shows excellent agreement between exact and numerical solution.

This test case can be used to verify first order convergence of the method. To this end, we simulate the solution at time $t = T/4$ on a $2^N \times 2^N$ grid using $15 \cdot 2^{N-5}$ time steps for $N = 5, \ldots, 9$. Table 3 gives the L^1 errors for each conserved quantity together with the corresponding convergence rates. The L^1 errors are computed according to a four point numerical quadrature and the convergence rates according to the formulae

$$\text{rate} = \log_2\left(\frac{\text{error}(\Delta x)}{\text{error}(\Delta x/2)}\right).$$

Although the transition from water to dry land is not smooth, the convergence rates are of order one in the L^1 norm.

TABLE 3. Errors and convergence rates in the conserved variables.

		L^1-error			rate		
grid	steps	h	hu	hv	h	hu	hv
32×32	15	0.8801	1.4311	0.8631	—	—	—
64×64	30	0.4192	0.6473	0.4381	1.07	1.14	0.98
128×128	60	0.2140	0.3272	0.2231	0.97	0.98	0.97
256×256	120	0.1090	0.1664	0.1137	0.97	0.98	0.97
512×512	240	0.0557	0.0864	0.0576	0.97	0.95	0.98

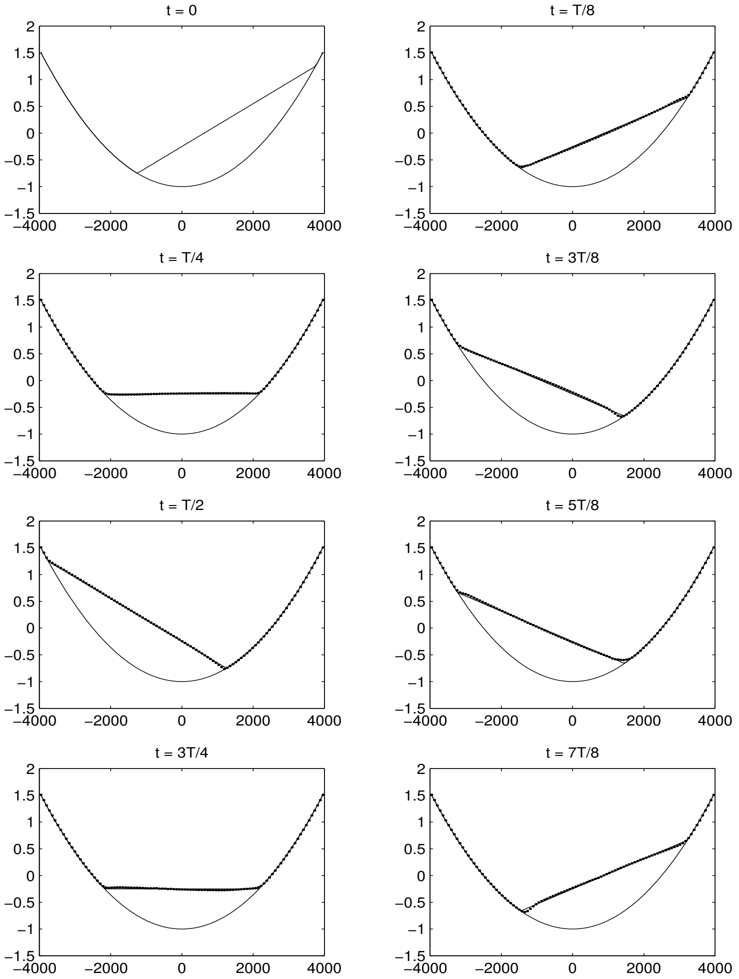

FIGURE 8. Front tracking solution along the plane $y = 0$ for oscillations in a parabolic basin. T denotes the period. The solid line represents the exact solution.

4.5. **Flow over an obstacle in one dimension.** In this example we study shallow water flow over a topography in one dimension. The initial boundary value problem is described in [19], where it is solved by the composite scheme LWLF4. The spatial interval is $x \in [-10, 10]$, and initial conditions are

$$h(x,0) + z_b(x) = 1.0, u(x,0) = 1.0,$$

with absorbing boundaries, and the bottom profile reads

$$z_b(x) = \begin{cases} 0.2\left(1 - \frac{x^2}{4}\right), & -2 \le x \le 2, \\ 0, & \text{otherwise.} \end{cases}$$

For the numerical computations we take $g = 1$.

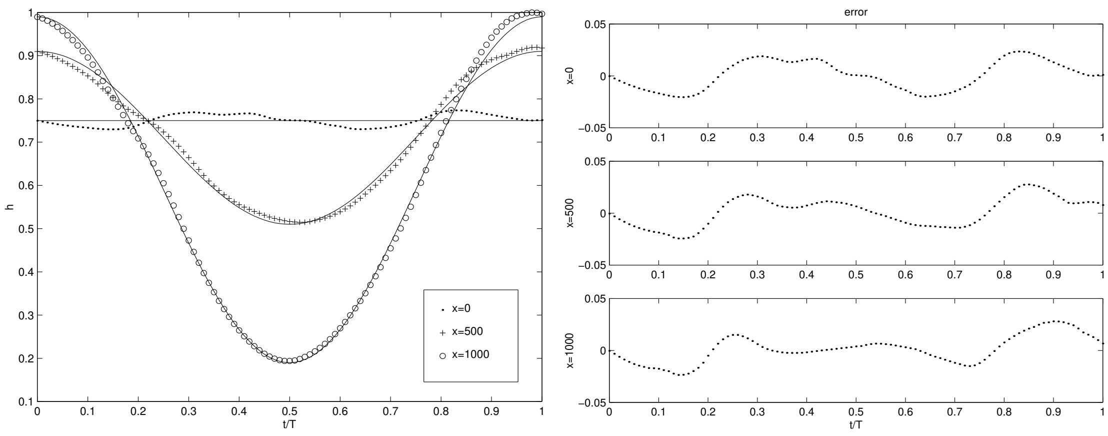

FIGURE 9. (Left) Water level at three different locations along the plane $y = 0$. (Right) Errors in the numerical solutions.

Operator splitting is used to handle the source term on the right hand side of the equations. The resulting homogeneous conservation law is solved by front tracking, while the ordinary differential equation is solved exactly. Because of the spatial dependency in the source term, it is natural to project the front tracking solution onto a (uniform) grid before adding the source term. In doing so, discontinuities in the solution are smeared. For shock waves, this introduces waves in the passive family, which may lead to post-shock oscillations (see [8]).

To amend this problem we introduce an adaptive grid. The wave type of each front is obtained as a byproduct from the Riemann solver and can be used as a monitor function for the adaptive strategy. In each projection we start with a given (uniform) grid. Then extra grid cells are included at the location of each shock front (or contact discontinuity for general systems) with strength exceeding a certain predefined threshold. This way strong discontinuities are tracked and post-shock oscillations are almost eliminated. Notice that this introduces hardly no computational overhead.

Solutions at times $t = 5$ and 10 computed with 100 and 2000 grid cells by front tracking with and without adaptive grid and LWLF4 are shown in Figure 10. The fixed CFL numbers used for front tracking and LWLF4 were 1.75 and 0.8, respectively. In the adaptive method, only two extra grid cells were added.

From the plots we see that front tracking without uniform grid needs only half as many points as LWLF4 to resolve the shock. By including adaptive grid, the shock waves are resolved exactly. For the rest of the solution the methods give approximately the same result.

5. DISCUSSION AND CONCLUSIONS

We have developed front tracking together with operator splitting as a numerical technique for the shallow water equations and tested it on four test cases.

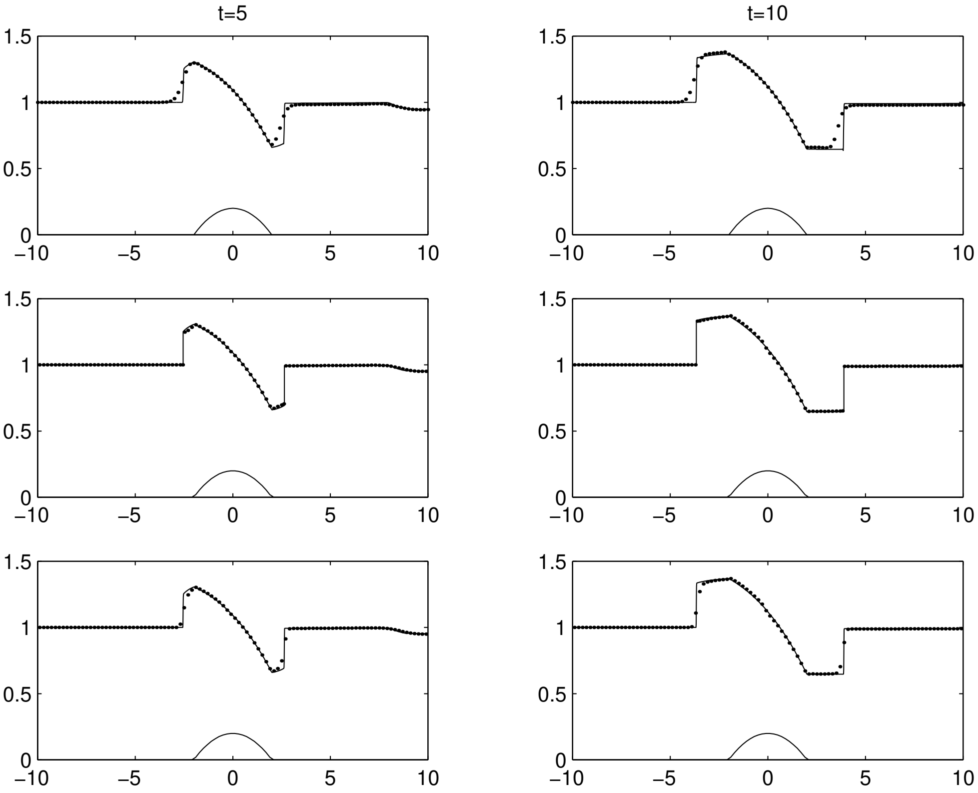

FIGURE 10. Shallow water flow over a topography in one-dimension computed by LWLF4 (top) and front tracking with (middle) and without (bottom) adaptive grid.

For hyperbolic equations time stepping should be governed by the dynamics, and, in particular, should be fairly independent of the spatial discretization. Front tracking is unconditionally stable in this sense. This increases the computational speed considerably. However, when used in conjunction with operator splitting one introduces errors due to the splitting as well as post-shock oscillations that effectively reduces the feasible CFL numbers to moderately above unity (i.e, typically in the interval 1–5). By construction the method resolves shocks very sharply. Grid refinement enhances the efficiency of the method, especially for the one-dimensional inhomogeneous problem.

Our experience shows that the first order front tracking method compares well with second order methods.

REFERENCES

[1] F. Alcrudo and P. Garcia-Navarro. A high-resolution Godunov-type scheme in finite volumes for the 2D shallow-water equations. *Internat. J. Numer. Methods Fluids*, 16:489–505, 1993.

[2] D. Ambrosi. Approximation of shallow water equations by Roe's Riemann solver. *Internat. J. Numer. Methods Fluids*, 20:157–168, 1995.

[3] A. Bermùdez, A. Dervieux, J. A. Désidéri, and M. E. Vázquez. Upwind schemes for the two-dimensional shallow water equations with variable depth using unstructured meshes. Rapport de recherche N^0 2738, INRIA, 1995.

[4] A. Bressan, G. Crasta, and B. Piccoli. Well-posedness of the Cauchy problem for $n \times n$ systems of conservation laws. *Mem. Amer. Math. Soc.* To appear.

[5] A. Bressan and P. LeFloch. Uniqueness of weak solutions to systems of conservation laws. *Arch. Rational Mech. Anal.*, 140(4):301–317, 1997.

[6] R. J. Fennema and M. H. Chaudhry. Explicit methods for 2-D transient free-surface flows. *J. Hydraul. Eng.*, 116:1013–1034, 1990.

[7] A. E. Gill. *Atmosphere–Ocean Dynamics.* Academic Press, New York, 1982.

[8] H. Holden, K.-A. Lie, and N. H. Risebro. A front tracking method for conservation laws in two dimensions. Preprint, Norwegian University of Science and Technology, 1998.

[9] H. Holden and N. H. Risebro. A method of fractional steps for scalar conservation laws without the CFL condition. *Math. Comp.*, 60(201):221–232, 1993.

[10] H. Holden and N. H. Risebro. Front Tracking for Conservation Laws. Department of Mathematics, Norwegian University of Science and Technology. Lecture Notes.

[11] G.-S. Jiang and E. Tadmor. Non-oscillatory central schemes for multidimensional hyperbolic conservation laws. Report 96-36, UCLA CAM, 1996. To appear in SIAM J. Sci. Comput. Available at the URL `http://www.math.ntnu.no/conservation/`.

[12] J. O. Langseth. On an implementation of a front tracking method for hyperbolic conservation laws. *Advances in Engineering Software*, 26(1):45–63, 1996.

[13] J. O. Langseth, N. H. Risebro, and A. Tveito. A conservative front tracking scheme for 1D hyperbolic conservation laws. In A. Donato and F. Oliveri, editors, *Nonlinear Hyperbolic Problems: Theoretical, Applied, and Computational Aspects (Taormina, 1992)*, volume 43 of *Notes Numer. Fluid Mech.*, pages 385–392. Vieweg, Braunschweig, 1993.

[14] R. J. LeVeque. CLAWPACK software. Available from `netlib.att.com` in `netlib/pdes/claw/` or at the URL `http://www.amath.washington.edu/~rjl/clawpack.html`.

[15] R. J. LeVeque. CLAWPACK User Notes. Applied Mathematics, Box 352420, University of Washington, Seattle, WA 98195–2420, Nov. 1995. Available from `netlib.att.com` in `netlib/pdes/claw/doc/` or at the URL `http://www.amath.washington.edu/~rjl/clawpack.html`.

[16] K.-A. Lie, V. Haugse, and K. H. Karlsen. Dimensional splitting with front tracking and adaptive grid refinement. *Numer. Methods Partial Differential Equations.* To appear.

[17] R. Liska, L. Margolin, and B. Wendroff. On nonhydrostatic two-layer models of incompressible flow. Preprint, 1996.

[18] R. Liska and B. Wendroff. Analysis and computation with multi-layer fluid models. Preprint, 1996.

[19] R. Liska and B. Wendroff. Composite schemes for conservation laws. To appear in SIAM J. Numer. Anal.

[20] R. Liska and B. Wendroff. 2D shallow water equations by composite schemes. Technical Report LAUR-97-4879, Los Alamos National Laboratories, Los Alamos, 1997.

[21] R. Liska and B. Wendroff. Analysis and computation with stratified fluid models. *J. Comp. Phys.*, 137:212–244, 1997.

[22] T.-P. Liu and J. Smoller. On the vacuum state for isentropic gas dynamics. *Adv. Pure Appl. Math.*, 1:345–359, 1980.

[23] A. T. Morel. *A Genuinely Multidimensional High-Resolution Scheme for the Shallow Water Equations.* PhD Thesis, Swiss Federal Institute of Technology, Zürich, 1997.

[24] A. N. Nazarov. Mathematical modeling of a snow-powder avalanche in the framework of the equations of two-layer shallow water. *Fluid Dynamics*, 26:70–75, 1991.

[25] N. H. Risebro. A front–tracking alternative to the random choice method. *Proc. Amer. Math. Soc*, 117(4):1125–1129, 1993.

[26] N. H. Risebro and A. Tveito. Front tracking applied to a nonstrictly hyperbolic system of conservation laws. *SIAM J. Sci. Stat. Comput.*, 12(6):1401–1419, 1991.
[27] N. H. Risebro and A. Tveito. A front tracking method for conservation laws in one dimension. *J. Comp. Phys.*, 101(1):130–139, 1992.
[28] W. C. Thacker. Some exact solutions to the nonlinear shallow-water wave equations. *J. Fluid Mech.*, 107:499–508, 1981.
[29] E. F. Toro. Riemann problems and the WAF method for solving the two-dimensional shallow water equations. *Philos. Trans. Roy. Soc. London Ser. A.*, 338:43–68, 1992.
[30] C. B. Vreugdenhil. Two-layer shallow-water flow in two dimensions, a numerical study. *J. Comput. Phys.*, 33:169–184, 1979.

(Runar Holdahl)
Department of Mathematical Sciences,
Norwegian University of Science and Technology,
N-7034 Trondheim, Norway

(Helge Holden)
Department of Mathematical Sciences,
Norwegian University of Science and Technology,
N-7034 Trondheim, Norway
E-mail address: `holden@math.ntnu.no`
URL: `http://www.math.ntnu.no/~holden/`

(Knut-Andreas Lie)
Department of Mathematical Sciences,
Norwegian University of Science and Technology,
N-7034 Trondheim, Norway
E-mail address: `andreas@math.ntnu.no`